10-1-2022

Oxygen Vacancies in LiB_3O_5 Crystals and Their Role in Nonlinear Absorption

Brian C. Holloway

Christopher A. Lenyk
Air Force Institute of Technology

Timothy D. Gustafson
Air Force Institute of Technology

Nancy C. Giles
Air Force Institute of Technology

Recommended Citation

B. C. Holloway, C. A. Lenyk, T. D. Gustafson, N. C. Giles, D. Perlov, and L. E. Halliburton, "Oxygen vacancies in LiB3O5 crystals and their role in nonlinear absorption," Opt. Mater. Express 12, 4155-4168 (2022)

Research Article Vol. 12, No. 10 / 1 Oct 2022 / Optical Materials Express 4155
Optical Materials EXPRESS

Oxygen vacancies in LiB_3O_5 crystals and their role in nonlinear absorption

B. C. HOLLOWAY,[1] C. A. LENYK,[1] T. D. GUSTAFSON,[1] N. C. GILES,[1] D. PERLOV,[2] AND L. E. HALLIBURTON[3,*]

[1]Department of Engineering Physics, Air Force Institute of Technology, Wright-Patterson Air Force Base, OH 45433, USA
[2]IPG Photonics Corporation, 50 Old Webster Road, Oxford, MA 01540, USA
[3]Department of Physics and Astronomy, West Virginia University, Morgantown, WV 26506, USA
*larry.halliburton@mail.wvu.edu

Abstract: LiB_3O_5 (LBO) crystals are used to generate the second, third, and fourth harmonics of near-infrared solid-state lasers. At high power levels, the material's performance is adversely affected by nonlinear absorption. We show that as-grown crystals contain oxygen and lithium vacancies. Transient absorption bands are formed when these intrinsic defects serve as traps for "free" electrons and holes created by x rays or by three- and four-photon absorption processes. Trapped electrons introduce a band near 300 nm and trapped holes produce bands in the 500-600 nm region. Electron paramagnetic resonance (EPR) is used to identify and characterize the electrons trapped at oxygen vacancies (the unpaired electron is localized on one neighboring boron). Self-trapped holes and lithium vacancies with the hole trapped on an adjacent oxygen are also observed with EPR. At room temperature, we predict that most of the unwanted defect-related ultraviolet absorption created by a short laser pulse will decay with a half-life of 29 μs.

1. Introduction

In many nonlinear optical materials, the maximum power that can be generated in the higher harmonics is often limited by nonlinear absorption. As stated by Röcker et al. [1], "Nonlinear absorption describes the phenomenon that two or more photons are absorbed at the same time which leads to an intensity-dependent absorption coefficient. This effect can occur when the sum of the photon energies is sufficient to overcome the energy gap between the valence and the conduction band of a material which otherwise would be transparent at the wavelength of interest." An increase in unwanted linear absorption is an important, and frequent, consequence of nonlinear absorption. Multiphoton processes (i.e., nonlinear absorption) can create discrete absorption bands within the energy gap by temporarily populating optically active charge states of point defects that are unintentionally present. When this happens, single-photon (i.e., linear) absorption may significantly increase at one or more of the wavelengths propagating through the crystal.

As expected, the formation of unwanted transient absorption bands associated with intrinsic point defects is recognized as a fundamental problem when lithium triborate (LiB_3O_5) crystals are used to generate the second, third, and fourth harmonics of near-infrared solid-state lasers [1–6]. The high pump powers used in these applications allow combinations of the harmonics to bridge the 7.7 eV bandgap of the crystals [7] and produce large numbers of free electrons and holes. In their recent study of LiB_3O_5 crystals, Röcker et al. [1] verified that four-photon absorption is the primary nonlinear absorption mechanism during second-harmonic generation and three-photon absorption is the dominant process during third-harmonic generation. Oxygen and lithium vacancies inadvertently present in the crystals serve as temporary traps for the free electrons and holes generated by the nonlinear absorption processes [8–13]. Self-trapped holes formed in the oxygen sublattice are also important participants [9].

#469756 https://doi.org/10.1364/OME.469756
Journal © 2022 Received 5 Jul 2022; revised 12 Sep 2022; accepted 13 Sep 2022; published 23 Sep 2022

Optical Materials EXPRESS

The oxygen and lithium vacancies are in nonparamagnetic charge states (V_O^{2+} and V_{Li}^{-}) in as-grown LiB_3O_5 crystals. To maintain charge neutrality, a crystal cannot have just one type of vacancy. Both types must be present, as they provide compensation for each other (two lithium vacancies compensate one oxygen vacancy). Exposing a crystal to ionizing radiation (x rays, in our case) allows free electrons and holes to be trapped and form localized defects having an unpaired spin. Electrons are trapped by oxygen vacancies and holes are either self-trapped on oxygen ions or are trapped at oxygen ions adjacent to a lithium vacancy. In the present study, electron paramagnetic resonance (EPR) is used to monitor these defects. Each charge state produced by the ionizing radiation has a distinct EPR spectrum [8–13] and is accompanied by an optical absorption band [8,11,14]. The trapped electrons are responsible for an absorption band peaking near 300 nm and the trapped holes have absorption bands in the 500-600 nm region. These defect-related transient absorption bands overlap the second and third harmonics of the infrared pump lasers. Activation energies obtained from the thermal decays of the trapped holes are used to predict lifetimes (at room temperature) of the unwanted transient absorption bands produced by the ionizing radiation, either intense laser beams or x rays. [Note: In this paper, we use "ionizing radiation" to mean any photons or combination of photons that bridge the energy gap of the crystal and produce electrons and holes in the conduction and valence bands, respectively. The x rays that we use and the third and fourth harmonics of high-powered infrared lasers are equivalent sources of ionizing radiation.]

A primary focus of our study is oxygen vacancies. In the earlier reports of defects in LiB_3O_5 crystals [8–13], little attention was directed toward these ubiquitous vacancies. Our present investigation identifies and characterizes optically active singly ionized oxygen vacancies and describes their central role in nonlinear absorption. Unintended effects of nonlinear absorption are often attributed to point defects [1–6], but it has proven difficult in the past to identify the specific defects involved. For example, are they intrinsic defects or impurities? We answer this question in the LiB_3O_5 crystals and anticipate that our results, and the methods we use, will be relevant for other nonlinear oxide crystals such as β-BaB_2O_4, where oxygen vacancies are known to be present [15].

2. Experimental details

The LiB_3O_5 crystals used in this study were grown at IPG Photonics (Oxford, MA) by the top-seeded solution growth method [16–18]. They represent currently available high quality commercial material, structurally perfect with very low impurity levels and low absorption. Figures 2, 3, 5, 6, and 7 in the present paper contain spectral data taken from these recently grown crystals. As expected, they show that the same defects observed many years earlier in Refs. [8–13] are still present in today's crystals.

Samples with dimensions of $2.3 \times 2.6 \times 3.0$ mm^3 were cut from larger boules. The crystals were irradiated with x rays from a Varian OEG-76H-Rh tube operating at 60 kV and 30 mA (irradiation times were two min). For low-temperature irradiations, the crystals were immersed in liquid nitrogen in a styrofoam cup. These x rays do not produce new vacancies: they only change the charge states of vacancies that had formed during growth. Using x rays, instead of the harmonics of lasers, allowed us to expose the entire volume of a crystal to intense ionizing radiation and thus maximize the concentrations of those charge states of the intrinsic defects that are responsible for unwanted absorption bands.

EPR spectra were taken with a Bruker EMX spectrometer operating near 9.4 GHz and an Oxford Instrument ESR-900 helium-gas flow system. Concentrations of EPR-active defects were obtained by making comparisons with a Bruker weak-pitch standard sample. The infrared absorption spectra of the OH^- ions were acquired with a ThermoScientific Nicolet 8700 FTIR spectrometer and a fused-silica wire-grid polarizer from Thorlabs (Model WP25M-UB). A Cryo

Optical Materials EXPRESS

Industries optical cryostat with sapphire windows (Model 110-637-DND) was used to maintain the sample temperature near 80 K during the infrared absorption measurements.

The LiB_3O_5 crystals are orthorhombic (space group $Pna2_1$) with two glide planes and one screw axis as symmetry elements [19–21]. Lattice constants at 20°C are $a = 8.444$ Å, $b = 7.378$ Å, and $c = 5.146$ Å. There are three inequivalent boron sites and five inequivalent oxygen sites in the crystal. All the lithium sites are equivalent. The LiB_3O_5 lattice contains both BO_3 and BO_4 units. As shown in Fig. 1, these units combine to form B_3O_7 anionic groups in the crystal (the labeling scheme in Ref. [19] is used). Two of the boron ions (B1 and B3) in the B_3O_7 group are threefold bonded and one boron ion (B2) is fourfold bonded. Five of the oxygen ions (O1, O2, O3, O4, and O5) lie close to the plane formed by the B1, B2, and B3 ions. Each lithium ion has four oxygen neighbors, and each oxygen ion has two boron neighbors. Four of the five oxygen ions also have a lithium neighbor (O1 is the only oxygen ion that does not have a close lithium ion). The Li-O separation distances vary from 1.986 to 2.172 Å, the B1-O and B3-O bond lengths range from 1.348 to 1.397 Å, and the B2-O bond lengths range from 1.461 to 1.487 Å.

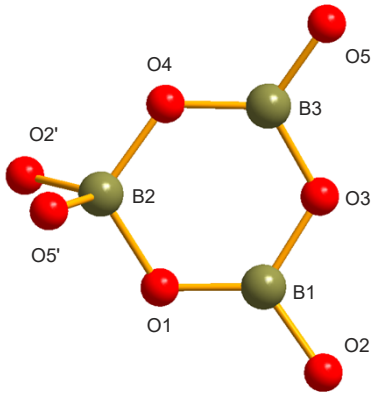

Fig. 1. Ball-and-stick illustration of the $(B_3O_7)^{5-}$ portion of the orthorhombic LiB_3O_5 crystal (arbitrarily oriented). The boron ions are green and the oxygen ions are red. The O2′ and O5′ ions are below and above the plane formed by the three boron ions.

3. Oxygen vacancies

Figure 2 shows the EPR spectrum produced in LiB_3O_5 by ionizing radiation. The crystal was initially exposed to x rays while being held at 77 K. Immediately after the irradiation, the crystal was quickly transferred from the liquid nitrogen to the cold helium gas flowing through the microwave resonator (there was minimal warming during the transfer). The spectrum in Fig. 2 was then taken at 55 K, with the magnetic field along the b axis and a microwave frequency of 9.395 GHz. This temperature is optimum for viewing the spectrum, as saturation effects due to long spin-lattice relaxation times decrease the intensity of the oxygen-vacancy lines at lower temperatures. Two paramagnetic defects are present in Fig. 2. The upper stick diagrams identify the strong ^{11}B lines and the weaker ^{10}B lines from the singly ionized oxygen vacancies (V_O^+). A lower stick diagram, with four closely spaced lines, identifies the self-trapped holes. The concentration of oxygen vacancies contributing to the spectrum is approximately 2.0×10^{17} cm^{-3}. Self-trapped holes appearing in the spectrum have a similar concentration. It is important to note that the EPR spectrum we are assigning to an oxygen vacancy [8–10] was attributed to interstitial B^{2+} ions in a series of early reports [11,13,22,23]. Our vacancy model is supported by an analysis of the spectrum's spin-Hamiltonian parameters (described later in this section) and by analogy with singly ionized oxygen vacancies in SiO_2 and TiO_2 crystals [24–26].

Optical Materials EXPRESS

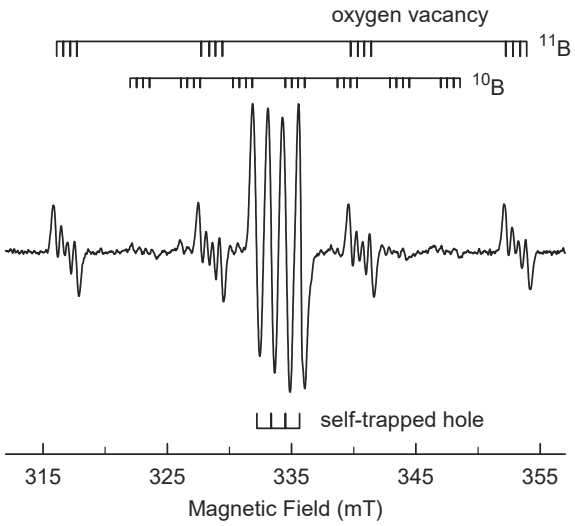

Fig. 2. EPR spectrum taken at 55 K after the LiB_3O_5 crystal was irradiated at 77 K with x rays. Lines from the singly ionized oxygen vacancy (V_O^+) are identified by the upper stick diagrams. Self-trapped holes are responsible for the four more intense, closely spaced lines in the center of the spectrum.

Oxygen vacancies in LiB_3O_5 crystals have two boron neighbors. An electron trapped by the vacancy is primarily localized on one of these two boron ions. This results in a large hyperfine interaction with one boron nucleus and a much weaker hyperfine interaction with the second boron nucleus (on the opposite side of the vacancy). The large interaction is responsible for the two sets of well separated EPR lines in Fig. 2 (from the ^{10}B and ^{11}B nuclei, respectively). The ^{10}B isotope is 19.9% abundant with $I = 3$ and the ^{11}B isotope is 80.1% abundant with $I = 3/2$. As the stick diagrams above the spectrum show, the large boron interaction gives four sets of ^{11}B lines with 12.08 mT separations and seven sets of ^{10}B lines with 4.05 mT separations. The number of sets of lines depends on the nuclear spin, with the $\Delta M_S = \pm 1$, $\Delta m_I = 0$ selection rules predicting $2I + 1$ sets of lines for an isotope. Our experimental value of 2.983 for the ratio of ^{10}B and ^{11}B separations in the V_O^+ spectrum in Fig. 2 agrees with the value of 2.986 predicted using the known spins and magnetic moments of the two boron isotopes. The weaker hyperfine interaction with the opposite (i.e., second) boron ion is responsible for the additional structure present on the sets of four and seven lines from the primary boron ion. These groups of four closely spaced lines with 0.53 mT separations represent a ^{11}B interaction (^{10}B lines are not resolved for this weaker interaction).

Figure 3 shows the angular dependence of the EPR spectrum from the V_O^+ centers. Only the primary ^{11}B interaction is plotted. Secondary splittings from the weak interaction with the second participating boron neighbor are not included. The direction of the magnetic field is rotated in three planes, from *a* to *b*, *b* to *c*, and *c* to *a*. For each plane, data were obtained for the outer lines (those at the highest and lowest magnetic fields). Significant overlap prevented accurate measurements of the positions of the inner sets of lines in each plane. The following spin-Hamiltonian, with electron Zeeman, hyperfine, and nuclear Zeeman terms, describes the angular dependence of the singly ionized oxygen vacancy.

$$H = \beta \mathbf{S} \cdot \mathbf{g} \cdot \mathbf{B} + \mathbf{I} \cdot \mathbf{A} \cdot \mathbf{S} - g_N \beta_N \mathbf{I} \cdot \mathbf{B} \quad (1)$$

There are four crystallographically equivalent orientations (often referred to as sites) for the V_O^+ center in the orthorhombic LiB_3O_5 lattice. Each of these four crystallographically equivalent

Optical Materials EXPRESS

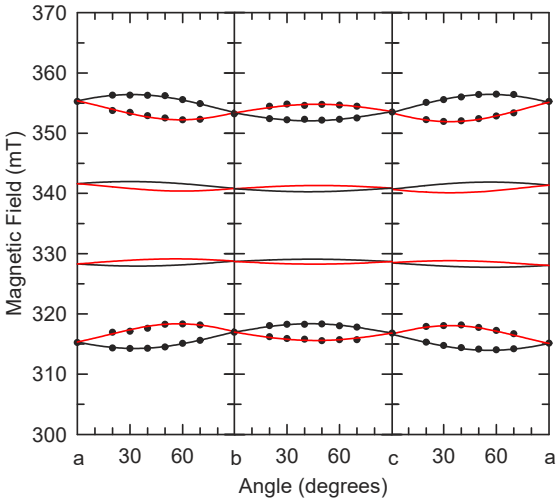

Fig. 3. Angular dependence of the EPR spectrum of singly ionized oxygen vacancies (V_O^+) in the *a*-*b*, *b*-*c*, and *c*-*a* planes. Discrete points are experimental, and the solid curves are calculated using the parameters in Table 1. Red curves identify the angular dependence of one of the four orientations of the V_O^+ defect.

orientations is a physically different orientation of the same defect. They are related to each other by the symmetry elements of the crystal. Each orientation of the defect has the same principal values for the **g** and **A** matrices. The principal-axis directions of these matrices, however, are different for each orientation. All four orientations are magnetically inequivalent for an arbitrary direction of the external magnetic field. They are pairwise degenerate when the magnetic field direction is in an *a*-*b*, *b*-*c*, or *c*-*a* plane and they are fourfold degenerate when the magnetic field direction is along *a*, *b*, or *c*. As expected, the angular dependence in Fig. 3 shows the pairwise degeneracy by splitting into two branches in each plane of rotation.

The **g** and **A** matrices in Eq. (1) each have, in general, six independent parameters. These are the three principal values and the three Euler angles that specify the directions of the principal axes. Rewriting the spin-Hamiltonian in matrix form provided an 8×8 matrix ($S = 1/2$ and $I = 3/2$ for the ^{11}B nuclei) that could be diagonalized to obtain the energy eigenvalues and the allowed transition energies. Values for the parameters were determined by performing these diagonalizations within a least-squares fitting program. Input data were the experimental magnetic-field positions in Fig. 3 and their corresponding microwave frequencies. Parameters were systematically varied until the predicted line positions agreed with the measured positions. Because of an arbitrary choice in site assignments, two sets of parameters gave equally good fits to the data taken in the three planes. This problem was resolved by comparing predicted spectra to experimental spectra obtained in a fourth plane, from *c* to the midpoint between *a* and *b*. The final correct set of parameters, for one orientation of the defect, are listed in Table 1. Red curves in Fig. 3 identify the EPR lines associated with this orientation. The fitting showed that the **g** and **A** matrices are both axial with only one principal axis direction (corresponding to the unique principal value) needed for each matrix. This reduced the number of independent parameters for each matrix from six to four. Polar and azimuthal angles (θ and ϕ) describe the directions for $g_{||}$ and $A_{||}$, where θ is defined relative to *c* and ϕ is defined relative to *a* with positive rotation being from *a* toward *b*. In Table 1, estimates of the uncertainties are ±0.0003 for the g values, ±2.0 MHz for the A values, and ±3° for the angles.

Optical Materials EXPRESS

Table 1. Spin-Hamiltonian parameters for the singly ionized oxygen vacancy.

g matrix	^{11}B hyperfine matrix
$g_\perp = 2.0016$	$A_\perp = 316.0$ MHz
$g_{\|\|} = 2.0007$	$A_{\|\|} = 415.8$ MHz
$\theta = 56.7°$	$\theta = 60.1°$
$\phi = 191.0°$	$\phi = 147.8°$

The experimentally determined principal values of the ^{11}B hyperfine matrix provide detailed information about the electronic structure of the singly ionized oxygen vacancy (V_O^+). This matrix can be written in the following form, where the parameters have physical meanings [27].

$$\mathbf{A} = \begin{pmatrix} \mathbf{A}_\perp & 0 & 0 \\ 0 & \mathbf{A}_\perp & 0 \\ 0 & 0 & \mathbf{A}_{||} \end{pmatrix} = \begin{pmatrix} a-b & 0 & 0 \\ 0 & a-b & 0 \\ 0 & 0 & a+2b \end{pmatrix} \tag{2}$$

In Eq. (2), a is the isotropic Fermi contact parameter and b is the anisotropic dipole-dipole parameter. Values for $A_\perp$ and $A_{||}$ in Table 1 give $a = 349.3$ MHz and $b = 33.3$ MHz. According to Fitzpatrick et al. [28], an electron occupying a boron 2p orbital has a value for b of 53.24 MHz (this is 2/5 of 133.10 MHz where 2/5 is the angular factor for p orbitals [29]). A comparison of the experimental and calculated values for b indicates that approximately 62.5% of the unpaired spin density for the V_O^+ center is in a 2p orbital on the primary boron neighbor. Also, according to Fitzpatrick et al. [28], an electron in a boron 2s orbital has a value of 2312.23 MHz for the Fermi contact parameter a. A comparison of our experimental value for a with this calculated value suggests that 15.1% of the unpaired spin density is in a 2s orbital on the neighboring boron. Together, our experimental results for a and b place 77.6% of the trapped electron in 2s and 2p orbitals on one boron ion neighboring the oxygen vacancy. The remaining 22.4% of the spin density is on the boron ion on the opposite side of the vacancy and on the oxygen ions that are neighbors to the primary boron ion. These results from the analysis of the EPR angular dependence are not consistent with the model of an interstitial B^{2+} ion [22]. In the as-grown crystal, a B^{3+} ion at an interstitial site would have a $1s^2$ configuration and, after trapping an electron, would become a B^{2+} ion with the $1s^2 2s$ configuration. This places the unpaired spin primarily in the 2s orbital of the interstitial boron ion, whereas our experimental results indicate that only 15.1% of the unpaired spin is in the 2s orbital on the central boron ion.

Based on our EPR results, we propose a defect model for the singly ionized oxygen vacancy (V_O^+) in LiB_3O_5 that has the unpaired spin localized in an sp^2 or sp^3 hybrid orbital extending out from a boron ion into the vacancy (which type of orbital depends on whether a threefold or fourfold bonded ion serves as the primary boron). Our model is analogous to the well-known singly ionized oxygen vacancy (referred to as the E_1' center) in α-quartz [24,25]. Feigl et al. [30] and others [31,32] have shown that highly asymmetric relaxations of the two cation neighbors cause the E_1' to have the unpaired spin localized on only one Si neighbor. In LiB_3O_5, we expect that a similar asymmetric relaxation of the two boron ions either side of the vacancy will occur. Other examples of Group VI vacancies (oxygen and selenium) having an electron localized on only one neighboring cation are found in TiO_2, $Li_2B_4O_7$, and $BaGa_4Se_7$ [26,33,34]. In contrast, singly ionized oxygen vacancies in cubic alkaline-earth oxides such as MgO have the unpaired electron symmetrically distributed over the six nearest-neighbor cations [35].

In addition to an EPR spectrum, the singly ionized oxygen vacancies (V_O^+) in LiB_3O_5 have a broad optical absorption band peaking near 300 nm. Figure 4 is taken from Ref. [8] and

Optical Materials EXPRESS

shows this absorption band. The spectrum in Fig. 4 was obtained at 90 K after irradiating the crystal at 90 K with x rays (there was no intervening warming). A 300 nm absorption band has also been observed immediately after an electron irradiation near 77 K [11,14]. The data in Fig. 4 were obtained under the same conditions as our EPR spectrum shown in Fig. 2. This EPR spectrum was briefly reported in Ref. [8], but the defect causing the electronlike signal was not identified at that time and, thus, the 300 nm band was not attributed to a specific defect. In the present investigation, our analysis of the angular dependence of the electronlike EPR spectrum demonstrates that oxygen vacancies are responsible. This, in turn, allows us to assign the 300 nm optical absorption band in LiB_3O_5 to singly ionized oxygen vacancies. Oxygen vacancies in many wide-bandgap materials have broad absorption bands peaking in the ultraviolet [35]. These include SiO_2 (212 nm), MgO (250 nm), $LiAlO_2$ (238 nm), and Al_2O_3 (255 nm) [36–39].

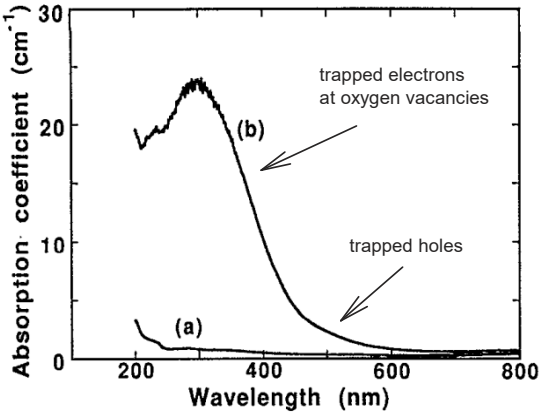

Fig. 4. Optical absorption spectra from a LiB_3O_5 crystal obtained at 90 K (a) before and (b) after an irradiation at 90 K with x rays. The large band peaking near 300 nm is assigned to singly ionized oxygen vacancies (V_O^+). A smaller unresolved band in the 500-600 nm region is due to trapped holes. Reproduced from M. P. Scripsick et al., J. Appl. Phys. **73**, 1114 (1993), with the permission of AIP Publishing.

4. Trapped holes

Self-trapped holes are an important defect in many oxide crystals [40–47]. They are typically stable only below 100 K and they require a distortion of the surrounding lattice to form the shallow potential well that serves as the trapping entity. As shown in Fig. 2, an EPR spectrum from self-trapped holes is produced in the LiB_3O_5 crystals by an irradiation at 77 K with x rays. Figure 5(a) is an expanded view of the middle portion of Fig. 2. The four lines with 1.20 mT spacings are the result of a hyperfine interaction with one ^{11}B nucleus. Spin-Hamiltonian parameters for this spectrum have been reported by Hong et al. [9]. In our present study, we extend the earlier work and obtain an activation energy describing the thermal decay of these defects. A model for the self-trapped hole, supported by unrestricted Hartree-Fock electronic structure calculations, was proposed in Ref. [9]. Referring to Fig. 1, this model has the hole localized in a nonbonding p orbital on the O4 oxygen ion with a large relaxation of the fourfold B2 ion back into the plane formed by the O1, O2′, and O5′ ions. The significant shift in position of the B2 ion produces the shallow potential well that allows self-trapping to occur.

Once formed by ionizing radiation (either the harmonics of lasers or x rays), the self-trapped holes in LiB_3O_5 are stable if the crystal remains below 90 K. Above this temperature, these holes become mobile (i.e., they are no longer self-trapped) and can migrate through the lattice. They either encounter a singly ionized oxygen vacancy and recombine with the trapped electron

Optical Materials EXPRESS

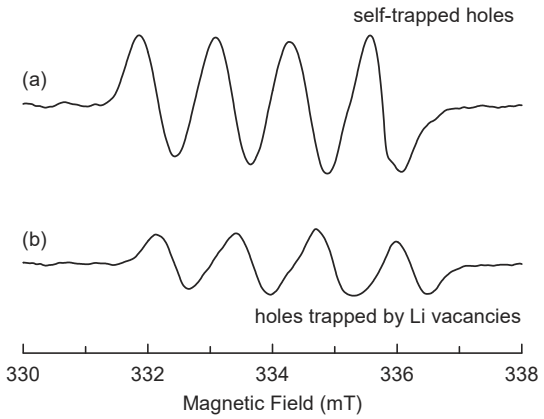

Fig. 5. (a) EPR spectrum from self-trapped holes, taken at 55 K after an irradiation at 77 K with x rays. (b) EPR spectrum from holes trapped by lithium vacancies, taken at 55 K after the irradiated crystal was warmed briefly to 100 K. The magnetic field is along the *b* direction and the microwave frequency is 9.395 GHz. Hyperfine with one ^{11}B nucleus is responsible for the four lines in each spectrum.

or they encounter a lithium vacancy (with an effective negative charge) and become trapped on an adjacent oxygen. This latter defect, the V_{Li}^{0} center, is electrically neutral. The EPR spectrum in Fig. 5(b) was taken at 55 K after holding the irradiated crystal at 100 K for several minutes. It shows the holes trapped by lithium vacancies. Hong et al. [9] also reported a set of spin-Hamiltonian parameters for this second trapped-hole defect. The spectra in Fig. 5 are similar, only distinguished by a small shift to higher field for the holes trapped by lithium vacancies. The concentration of self-trapped holes in Fig. 5(a) is 2.0×10^{17} cm^{-3}, and the concentration of holes trapped by lithium vacancies in Fig. 5(b) is 7.2×10^{16} cm^{-3}. Nearly two-thirds of the initial self-trapped holes recombined with trapped electrons during the 100 K warming step. A further warming step to 160 K destroyed the holes trapped by lithium vacancies. An EPR spectrum taken at 55 K after holding the crystal at 160 K for several minutes showed that all the trapped holes had thermally decayed.

At the temperatures where the self-trapped holes and the holes trapped by lithium vacancies become thermally unstable (100 and 160 K), there are corresponding decreases in the number of electrons trapped at oxygen vacancies. Estimates of the activation energies describing the thermal release of these holes, and thus the removal of the optical absorption bands associated with the trapped electrons and holes, are obtained by using the approximation $E \approx 25kT_m$ from the thermoluminescence community [48–51]. Here, T_m represents the decay temperature of a defect. Values of 100 and 160 K for T_m give activation energies of 0.22 and 0.34 eV for the self-trapped holes and the holes trapped by lithium vacancies. Uncertainties are ±0.01 eV. The singly ionized oxygen vacancies with a deep (2+/+) level are expected to decay at temperatures higher than the trapped hole centers. They do not survive to the higher temperatures, however, because they are destroyed when the released holes recombine with the trapped electrons.

The trapped holes in LiB_3O_5 are part of the large family of acceptor-bound small polarons. Unlike the trapped electrons with an optical absorption band in the ultraviolet, the trapped holes have absorption bands in the visible region of the spectrum. Schirmer [52], in a comprehensive review of holelike small polarons in oxides, has shown that these defects typically have broad absorption bands peaking near 550 nm. With this guidance, we assign the small unresolved band in the 500-600 nm region in Fig. 4 to the trapped holes produced by the x rays. Differences in the intensities of the bands at 300 nm and in the 500-600 nm region in this figure are due to

Optical Materials EXPRESS

different oscillator strengths, since the trapped electrons and trapped holes responsible for the two bands have similar concentrations. Absorption bands from singly ionized oxygen vacancies have oscillator strengths near 0.8 [35], whereas absorption bands from trapped hole centers typically have oscillator strengths near or less than 0.1 [52].

5. Additional defects involving lithium vacancies

We have encountered two additional defects that provide evidence for lithium vacancies in as-grown LiB_3O_5 crystals. The first of these is an OH^- ion adjacent to a lithium vacancy and the second is a Cu^{2+} ion substituting for a Li^+ ion with a nearby lithium vacancy. In each case, the resulting complex is electrically neutral. Hydrogen and copper are present at trace levels in some LiB_3O_5 crystals and are not detectable in other crystals.

Figure 6 shows the infrared absorption peak from OH^- ions in an as-grown LiB_3O_5 crystal. This absorption band was initially reported in 1997 by Kovács et al. [53] and is now seen in recently grown crystals. At 80 K, the band peaks at 3460.7 cm^{-1} and the width measured at the half-maximum points is 1 cm^{-1}. This band can be seen at room temperature, but with greatly reduced intensity because of an increase of the width to 10 cm^{-1}. In Fig. 6, we show that the absorption band is strongly polarized with the greatest intensity with E || *b* and a much smaller intensity with E || *a*. The band was not seen in spectra taken with E || *c*. Because the oscillator strength of OH^- ions has not been established in LiB_3O_5 [54,55], an estimate is not made of the OH^- concentration in Fig. 6. We assign the 3460.7 cm^{-1} infrared absorption peak in LiB_3O_5 to an OH^- ion occupying one of the four oxygen sites next to a lithium vacancy. Wöhlecke and Kovács [55], in their review article, have shown that OH^- ions in oxides are often adjacent to an intrinsic charge-compensating acceptor defect (e.g., a cation vacancy).

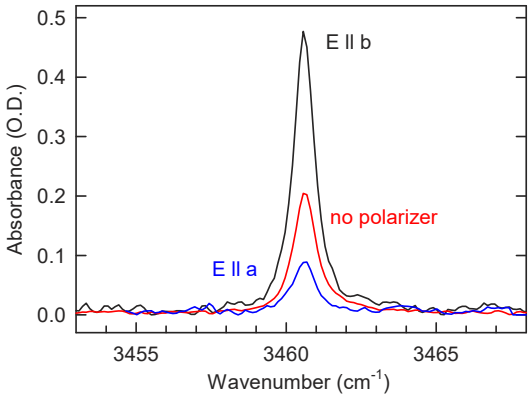

Fig. 6. Infrared absorption spectrum from OH^- molecular ions in a LiB_3O_5 crystal, taken at 80 K with light propagating along the *c* direction. This polarized band peaking at 3460.7 cm^{-1} is assigned to OH^- ions adjacent to lithium vacancies.

Figure 7 shows the EPR spectrum from Cu^{2+} ($3d^9$) ions that occupy a lithium site and have a nearby lithium vacancy. These data were taken at 55 K from a LiB_3O_5 crystal that had been irradiated at room temperature with x rays. The magnetic field is along the *c* direction and the microwave frequency is 9.394 GHz. Allowed lines from the ^{63}Cu and ^{65}Cu isotopes are identified by the stick diagrams above the spectrum. Less intense forbidden transitions appear between the lower two lines and between the upper two lines. The concentration of Cu^{2+} ions in Fig. 7 is 1.3×10^{16} cm^{-3}. These impurities very likely entered the crystal from the starting materials used in the growth.

Optical Materials EXPRESS

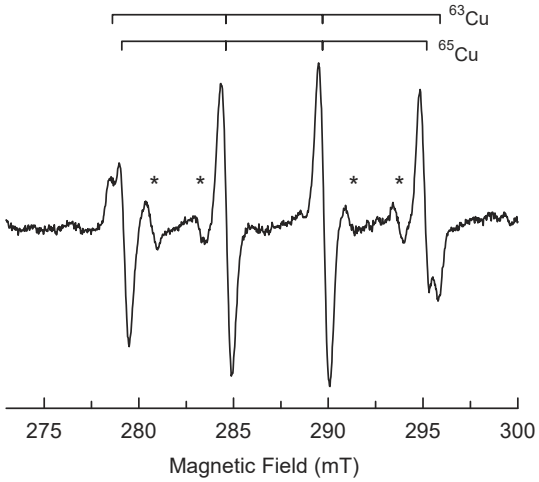

Fig. 7. EPR spectrum from Cu^{2+} ions in LiB_3O_5, taken at 55 K after an irradiation at room temperature with x rays. Stick diagrams identify the primary "allowed" ^{63}Cu and ^{65}Cu lines. Smaller lines marked by asterisks (*) are forbidden transitions.

Ryadun et al. [56] initially reported this Cu^{2+} EPR spectrum. Soon after, Kananen et al. [57] observed the same spectrum in a Cu-diffused LiB_3O_5 crystal and suggested that the model was Cu^{2+} ions perturbed by a nearby lithium vacancy. In the as-grown LiB_3O_5 crystal used in Fig. 7, nonparamagnetic Cu^{+} ($3d^{10}$) ions are near lithium vacancies. Then, during an irradiation at room temperature, they trap holes and become paramagnetic Cu^{2+} ions. For the crystal to remain electrically neutral, a corresponding number of electrons are trapped at oxygen vacancies and form V_O^+ centers with the unwanted 300 nm absorption band. This mechanism, where ionizing radiation (lasers or x rays) results in holes trapped at transition-metal impurities and electrons trapped at oxygen vacancies, will produce linear absorption that is stable at room temperature. In as-grown crystals, transition-metal impurities may also directly contribute to visible and near-ultraviolet absorption via their d-d transitions. It is, however, difficult to incorporate many of the transition-metal ions in LiB_3O_5 crystals because of size and/or charge misfits with Li^+ and B^{3+} ions.

6. Lifetimes of optical absorption bands

In an informative study of LiB_3O_5 crystals, Ogorodnikov et al. [14] used 7 ns pulses of 150 keV electrons to produce the same ionizing effects as intense laser beams. They found that stable optical absorption bands with peaks near 300 nm and 550 nm were produced at 77 K by the high-energy electrons. The same optical absorption bands were produced at room temperature by a single pulse of electrons, and quickly decayed after the pulse. At 295 K, there are two decay steps in the time response of the transient optical absorption (see Fig. 3 in Ref. [14]), one near 33 μs which accounts for approximately 83% of the initial absorption and the other near 2 ms which accounts for the remaining 17% of the initial absorption. Based on our results in the present study, we attribute these two steps to the thermal decay of the self-trapped holes and the holes trapped by lithium vacancies, respectively. Thermal release of these holes will destroy the 300 nm absorption as holes move to singly ionized oxygen vacancies (V_O^+) and recombine with the trapped electrons. In Section 4, values for the thermal activation energies describing the release of the holes from the two trapping sites were estimated to be 0.22 and 0.34 eV. These values allow

Optical Materials EXPRESS

us to predict decay times that can be compared to the pulsed electron results of Ogorodnikov et al. [14].

We use second-order kinetics, represented by Eq. (3), to describe the thermal decay of the self-trapped holes [58,59]. A second-order kinetics approach is appropriate when retrapping is likely to occur. It is used here because, after a self-trapped hole is released, it has a significant probability of being retrapped, maybe more than once, before reaching an oxygen vacancy.

$$\frac{dn}{dt} = -s'n^2 \exp\left(-\frac{E}{kT}\right). \tag{3}$$

In Eq. (3), n is the concentration of self-trapped holes with units of cm^{-3}, s' is a pre-exponential factor with units of $cm^3 s^{-1}$, and E is the activation energy. With n_0 being the concentration when $t = 0$, the solution to Eq. (3) is the hyperbolic decay function

$$n = \frac{n_0}{1 + at}, \tag{4}$$

where

$$a = n_0 s' \exp\left(-\frac{E}{kT}\right). \tag{5}$$

The half-life of the decay is a^{-1}. This is the time required for half of the self-trapped holes to be thermally destroyed after a pulse of ionizing radiation. At 295 K, $E = 0.22$ eV and $n_0 s' = 2 \times 10^8$ s^{-1} gives a value of 29 μs for the half-life. This predicted value obtained directly from the thermal stability of the self-trapped holes agrees with the experimental value of 33 μs reported by Ogorodnikov et al. [14] for the first, and largest, decay step of their induced ultraviolet absorption following a pulse of high-energy electrons. Repeating the calculation for the room-temperature half-life of the holes trapped by lithium vacancies, where $E = 0.34$ eV, gives 3.2 ms. This result is close to the value of 2 ms found by Ogorodnikov et al. [14] for the second decay step. Retrapping will play less of a role in the decay of the holes trapped by the lithium vacancies, and the use of Eq. (3) is expected to provide a lifetime that is too long. The general agreement of the predicted and experimental values for the two half-lives demonstrates a consistency with other studies [14] and strongly supports our explanations of the physical mechanisms responsible for defect-related effects of nonlinear absorption in LiB_3O_5 crystals.

7. Summary

Lithium triborate (LiB_3O_5) crystals contain oxygen and lithium vacancies, with concentrations approaching 1 ppm. In the as-grown crystals, these vacancies are in nonparamagnetic charge states and do not have associated optical absorption bands. When a LiB_3O_5 crystal is exposed at 77 K to ionizing radiation (we use x rays instead of the harmonics from lasers), singly ionized oxygen vacancies and self-trapped holes are formed. These defects are thermally stable at 77 K and are easily seen with electron paramagnetic resonance (EPR). The electrons trapped at the oxygen vacancies are responsible for a broad absorption band peaking near 300 nm and the trapped holes contribute to absorption in the 500-600 nm region. In the present paper, these V_O^+ oxygen vacancies are fully characterized. Their production conditions and decay mechanisms are determined, and a complete set of spin-Hamiltonian parameters are obtained from the angular dependence of the EPR spectrum. Using these parameters, we establish the electronic structure of the V_O^+ centers and construct a model.

When the temperature of the crystal is increased after the irradiation, the self-trapped holes become thermally unstable near 100 K and either recombine with an electron at an oxygen vacancy or become trapped at an oxygen ion adjacent to a lithium vacancy (thus forming V_{Li}^0 centers). The holes trapped by the lithium vacancies are slightly more stable and decay when

Optical Materials EXPRESS

the crystal is warmed to 160 K. At each decay step, electrons trapped at oxygen vacancies are annihilated by mobile holes and the unwanted V_O^+ optical absorption band at 300 nm decreases. From these decay temperatures, 100 and 160 K, activation energies of 0.22 eV and 0.34 eV, respectively, are obtained for the thermal release of holes from the trapping sites.

The ultraviolet and visible absorption bands associated with these trapped electrons and holes are short-lived at room temperature. Using the 0.22 eV activation energy obtained from the thermal decay of the self-trapped holes, we predict that most of the unwanted optical absorption produced by the higher harmonics of infrared lasers will decay at room temperature with a half-life of 29 μs. The remaining much smaller amount of unwanted absorption, present because of the holes trapped at lithium vacancies, will decay at room temperature with a half-life of 2 to 3 ms.

8. Future directions

Our present study describes a mechanism by which intrinsic defects (vacancies), and not impurities, are the main contributor to nonlinear absorption in commercially available LiB_3O_5 crystals. These results suggest that efforts by crystal growers to minimize nonlinear absorption should concentrate on maintaining stoichiometry, either during growth or with post-growth treatments that add lithium and/or oxygen ions. Also, we recognize that a more complete understanding of nonlinear absorption will emerge from studies using pulsed lasers to induce ultraviolet absorptions and measure decay times. Our predicted absorption lifetimes can be tested in these experiments. Finally, our results are expected to stimulate advanced density-functional-theory (DFT) computational studies that explore the electronic structure of oxygen vacancies and free and bound small polarons in LiB_3O_5 crystals (i.e., their charge states, lattice relaxations, thermal stabilities, hyperfine parameters, and the strengths and positions of optical absorption bands).

Funding. National Research Council.

Acknowledgments. Timothy D. Gustafson was supported at the Air Force Institute of Technology by a Research Associateship Award from the National Research Council (NRC). Any opinions, findings, and conclusions or recommendations expressed in this paper are those of the authors and do not necessarily reflect the views of the United States Air Force.

Disclosures. The authors declare no conflicts of interest.

Data Availability. Data underlying the results presented in this paper are not publicly available at this time but may be obtained from the authors upon reasonable request.

References

1. C. Röcker, P. Weinert, P. Villeval, D. Lupinski, M. Delaigue, C. Hönninger, R. Weber, T. Graf, and M. A. Ahmed, "Nonlinear absorption in lithium triborate frequency converters for high-power ultrafast lasers," Opt. Express **30**(4), 5423–5438 (2022).
2. C. Mühlig and S. Bublitz, "Characterization of nonlinear optical crystal absorption," Opt. Eng. **57**(12), 1 (2018).
3. O. I. Vershinin, A. V. Konyashkin, and O. A. Ryabushkin, "Anisotropy of nonlinear optical absorption of LBO crystals at 355 nm," Opt. Lett. **43**(1), 58–61 (2018).
4. D. G. Nikitin, O. A. Byalkovskiy, O. I. Verhinin, P. V. Puyu, and V. A. Tyrtyshnyy, "Sum frequency generation of UV laser radiation at 266 nm in LBO crystal," Opt. Lett. **41**(7), 1660–1663 (2016).
5. M. Takahashi, G. Masada, I. Sekine, M. Cadatal, T. Shimizu, N. Sarukura, C. Byeon, V. Fedorov, S. Mirov, A. Dergachev, and P. F. Moulton, "Reduction of nonlinear absorption in $Li_2B_4O_7$ by temperature- and repetition rate-control," Jpn. J. Appl. Phys. **48**(11), 112502 (2009).
6. N. Wang, J. Zhang, H. Yu, X. Lin, and G. Yang, "Sum-frequency generation of 133 mJ, 270 ps laser pulses at 266 nm in LBO crystals," Opt. Express **30**(4), 5700–5708 (2022).
7. Z. Hu, Y. Zhao, Y. Yue, and X. Yu, "Large LBO crystal growth at 2 kg-level," J. Cryst. Growth **335**(1), 133–137 (2011).
8. M. P. Scripsick, X. H. Fang, G. J. Edwards, L. E. Halliburton, and J. K. Tyminski, "Point defects in lithium triborate (LiB_3O_5) crystals," J. Appl. Phys. **73**(3), 1114–1118 (1993).
9. W. Hong, M. M. Chirila, N. Y. Garces, L. E. Halliburton, D. Lupinski, and P. Villeval, "Electron paramagnetic resonance and electron-nuclear double resonance study of trapped-hole centers in LiB_3O_5 crystals," Phys. Rev. B **68**(9), 094111 (2003).

Optical Materials EXPRESS

10. W. Hong, N. Y. Garces, M. M. Chirila, and L. E. Halliburton, "Identification of point defects responsible for laser-induced ultraviolet absorption in LiB_3O_5 (LBO) crystals," Proc. SPIE **4932**, 309–318 (2003).
11. I. N. Ogorodnikov, A. Y. Kuznetsov, A. V. Kruzhalov, and V. A. Maslov, "Point defects and short-wavelength luminescence of LiB_3O_5 single crystals," Radiat. Eff. Defects Solids **136**(1-4), 233–237 (1995).
12. A. V. Porotnikov, I. N. Ogorodnikov, S. V. Kudyakov, A. V. Kruzhalov, and S. L. Votyakov, "EPR of hole centers in nonlinear LiB_3O_5 crystals," Phys. Solid State **39**(8), 1224–1227 (1997).
13. I. N. Ogorodnikov, L. I. Isaenko, A. V. Kruzhalov, and A. V. Porotnikov, "Thermally stimulated luminescence and lattice defects in crystals of alkali metal borate LiB_3O_5 (LBO)," Radiat. Meas. **33**(5), 577–581 (2001).
14. I. N. Ogorodnikov, A. V. Kruzhalov, A. V. Porotnikov, and V. Y. Yakovlev, "Dynamics of electronic excitations and localized states in LiB_3O_5," J. Lumin. **76-77**, 464–466 (1998).
15. W. Hong, L. E. Halliburton, K. T. Stevens, D. Perlov, G. C. Catella, R. K. Route, and R. S. Feigelson, "Electron paramagnetic resonance study of electron and hole traps in β-BaB_2O_4 crystals," J. Appl. Phys. **94**(4), 2510–2515 (2003).
16. I. Nikolov, D. Perlov, S. Livneh, E. Sanchez, P. Czechowicz, V. Kondilenko, and D. Loiacono, "Growth and morphology of large LiB_3O_5 single crystals," J. Cryst. Growth **331**(1), 1–3 (2011).
17. N. A. Pylneva, N. G. Kononova, A. M. Yurkin, G. G. Bazarova, and V. I. Danilov, "Growth and nonlinear optical properties of lithium triborate crystals," J. Cryst. Growth **198-199**, 546–550 (1999).
18. H. G. Kim, J. K. Kang, S. H. Lee, and S. J. Chung, "Growth of lithium triborate crystals by the TSSG technique," J. Cryst. Growth **187**(3-4), 455–462 (1998).
19. S. F. Radaev, B. A. Maximov, V. I. Simonov, B. V. Andreev, and V. A. D'yakov, "Deformation density in lithium triborate, LiB_3O_5," Acta Crystallogr., Sect. B: Struct. Sci. **48**(2), 154–160 (1992).
20. C. Le Hénaff, N. K. Hansen, J. Protas, and G. Marnier, "Electron density distribution in LiB_3O_5 at 293 K," Acta Crystallogr., Sect. B: Struct. Sci. **53**(6), 870–879 (1997).
21. Y. F. Shepelev, R. S. Bubnova, S. K. Filatov, N. A. Sennova, and N. A. Pilneva, "LiB_3O_5 crystal structure at 20, 227 and 377°C," J. Solid State Chem. **178**(10), 2987–2997 (2005).
22. A. Y. Kuznetsov, A. B. Sobolev, I. N. Ogorodnikov, and A. V. Kruzhalov, "Modeling of paramagnetic B^{2+} center in lithium triborate," Phys. Solid State **36**(12), 1876–1879 (1994).
23. I. N. Ogorodnikov, V. I. Kirpa, A. V. Kruzhalov, and A. V. Porotnikov, "Thermally stimulated emission of electrons and photons in nonlinear LiB_3O_5 crystals," Tech. Phys. **42**(7), 832–836 (1997).
24. R. H. Silsbee, "Electron spin resonance in neutron-irradiated quartz," J. Appl. Phys. **32**(8), 1459–1462 (1961).
25. M. G. Jani, R. B. Bossoli, and L. E. Halliburton, "Further characterization of the E_1' center in crystalline SiO_2," Phys. Rev. B **27**(4), 2285–2293 (1983).
26. A. T. Brant, N. C. Giles, S. Yang, M. A. R. Sarker, S. Watauchi, M. Nagao, I. Tanaka, D. A. Tryk, A. Manivannan, and L. E. Halliburton, "Ground state of the singly ionized oxygen vacancy in rutile TiO_2," J. Appl. Phys. **114**(11), 113702 (2013).
27. J.-M. Spaeth, J. R. Niklas, and R. H. Bartram, *Structural Analysis of Point Defects in Solids: An Introduction to Multiple Magnetic Resonance Spectroscopy* (Springer-Verlag, 1992), pp. 53–56.
28. J. A. J. Fitzpatrick, F. R. Manby, and C. M. Western, "The interpretation of molecular magnetic hyperfine interactions," J. Chem. Phys. **122**(8), 084312 (2005).
29. J. R. Morton and K. F. Preston, "Atomic parameters for paramagnetic resonance data," J. Magn. Reson. **30**(3), 577–582 (1978).
30. F. J. Feigl, W. B. Fowler, and K. L. Yip, "Oxygen vacancy model for the E_1' center in SiO_2," Solid State Commun. **14**(3), 225–229 (1974).
31. M. Boero, A. Pasquarello, J. Sarnthein, and R. Car, "Structure and hyperfine parameters of E_1' centers in α-quartz and in vitreous SiO_2," Phys. Rev. Lett. **78**(5), 887–890 (1997).
32. C. J. Pickard and F. Mauri, "First-principles theory of the EPR g tensor in solids: defects in quartz," Phys. Rev. Lett. **88**(8), 086403 (2002).
33. M. W. Swinney, J. W. McClory, J. C. Petrosky, S. Yang, A. T. Brant, V. T. Adamiv, Y. V. Burak, P. A. Dowben, and L. E. Halliburton, "Identification of electron and hole traps in lithium tetraborate ($Li_2B_4O_7$) crystals: oxygen vacancies and lithium vacancies," J. Appl. Phys. **107**(11), 113715 (2010).
34. B. C. Holloway, T. D. Gustafson, C. A. Lenyk, N. C. Giles, K. T. Zawilski, P. G. Schunemann, K. L. Averett, and L. E. Halliburton, "Optically active selenium vacancies in $BaGa_4Se_7$ crystals," J. Appl. Phys. **130**(17), 173104 (2021).
35. B. Henderson, "Anion vacancy centers in alkaline-earth oxides," Crit. Rev. Solid State Mater. Sci. **9**(1), 1–60 (1980).
36. R. A. Weeks and E. Sonder, "The relation between the magnetic susceptibility, electron spin resonance, and optical absorption of the E_1' center in fused silica," in *Paramagnetic Resonance*, Vol. II, edited by W. Low, (Academic Press, 1963), page 869.
37. L. A. Kappers, R. L. Kroes, and E. B. Hensley, "F^+ and F' centers in magnesium oxide," Phys. Rev. B **1**(10), 4151–4157 (1970).
38. M. S. Holston, I. P. Ferguson, J. W. McClory, N. C. Giles, and L. E. Halliburton, "Oxygen vacancies in $LiAlO_2$ crystals," Phys. Rev. B **92**(14), 144108 (2015).
39. B. D. Evans and M. Stapelbroek, "Optical properties of the F^+ center in crystalline Al_2O_3," Phys. Rev. B **18**(12), 7089–7098 (1978).

Optical Materials EXPRESS

40. A. M. Stoneham, J. Gavartin, A. L. Shluger, A. V. Kimmel, D. M. Ramo, H. M. Rønnow, G. Aeppli, and C. Renner, "Trapping, self-trapping and the polaron family," J. Phys.: Condens. Matter **19**(25), 255208 (2007).
41. T. E. R. Dodson, L. E. Halliburton, G. S. Kedziora, C. A. Lenyk, and N. C. Giles, "Self-trapped holes (small polarons) in ferroelectric KH_2PO_4 crystals," J. Phys.: Condens. Matter **31**(50), 505503 (2019).
42. W. Traiwattanapong, A. Janotti, N. Umezawa, S. Limpijumnong, J. T-Thienprasert, and P. Reunchan, "Self-trapped holes in $BaTiO_3$," J. Appl. Phys. **124**(8), 085703 (2018).
43. V. Laguta, M. Buryi, J. Pejchal, V. Babin, and M. Nikl, "Hole self-trapping in $Y_3Al_5O_{12}$ and $Lu_3Al_5O_{12}$ garnet crystals," Phys. Rev. Appl. **10**(3), 034058 (2018).
44. B. E. Kananen, N. C. Giles, L. E. Halliburton, G. K. Foundos, K. B. Chang, and K. T. Stevens, "Self-trapped holes in β-Ga_2O_3 crystals," J. Appl. Phys. **122**(21), 215703 (2017).
45. S. Yang, A. T. Brant, and L. E. Halliburton, "Photoinduced self-trapped hole center in TiO_2 crystals," Phys. Rev. B **82**(3), 035209 (2010).
46. V. V. Laguta, M. Nikl, J. Rosa, B. V. Grinyov, L. L. Nagornaya, and I. A. Tupitsina, "Electron spin resonance study of self-trapped holes in $CdWO_4$ scintillator crystals," J. Appl. Phys. **104**(10), 103525 (2008).
47. D. L. Griscom, "Self-trapped holes in amorphous silicon dioxide," Phys. Rev. B **40**(6), 4224–4227 (1989).
48. J. T. Randall and M. H. F. Wilkins, "Phosphorescence and electron traps I. The study of trap distributions," Proc. R. Soc. Lond. A **184**(999), 365–389 (1945).
49. A. G. Milnes, *Deep Impurities in Semiconductors* (John Wiley and Sons, 1973), Chap. 9, pp. 227–228.
50. T. D. Gustafson, N. C. Giles, B. C. Holloway, C. A. Lenyk, J. Jesenovec, J. S. McCloy, M. D. McCluskey, and L. E. Halliburton, "Cu^{2+} and Cu^{3+} acceptors in β-Ga_2O_3 crystals: A magnetic resonance and optical absorption study," J. Appl. Phys. **131**(6), 065702 (2022).
51. Y. Jiang, N. C. Giles, and L. E. Halliburton, "Persistent photoinduced changes in charge states of transition-metal donors in hydrothermally grown ZnO crystals," J. Appl. Phys. **101**(9), 093706 (2007).
52. O. F. Schirmer, "O^- bound small polarons in oxide materials," J. Phys.: Condens. Matter **18**(43), R667–R704 (2006).
53. L. Kovács, K. Polgár, A. Péter, and R. Capelletti, "FT-IR spectroscopy of OH^- ions in borate single crystals," Mikrochim. Acta [Suppl.] **14**, 523–524 (1997).
54. M. Stavola and W. B. Fowler, "Tutorial: Novel properties of defects in semiconductors revealed by their vibrational spectra," J. Appl. Phys. **123**(16), 161561 (2018).
55. M. Wöhlecke and L. Kovács, "OH^- ions in oxide crystals," Crit. Rev. Solid State Mater. Sci. **26**(1), 1–86 (2001).
56. AA Ryadun, V. A. Nadolinny, O. V. Antonova, and M. I. Rakhmanova, "Impurity and radiation defects in LiB_3O_5 crystals: the nature of centers in LiB_3O_5 crystals which are responsible for coloration during the long-term operation of optical elements," J. Struct. Chem. **58**(5), 885–892 (2017).
57. B. E. Kananen, J. W. McClory, N. C. Giles, and L. E. Halliburton, "Copper-doped lithium triborate (LiB_3O_5) crystals: A photoluminescence, thermoluminescence, and electron paramagnetic resonance study," J. Lumin. **194**, 700–705 (2018).
58. R. Chen, D. J. Huntley, and G. W. Berger, "Analysis of thermoluminescence data dominated by second-order kinetics," Phys. Stat. Sol. (a) **79**(1), 251–261 (1983).
59. R. Chen and S. W. S. McKeever, *Theory of Thermoluminescence and Related Phenomena* (World Scientific Publishing Co., 1997), pp. 29–33.